Electronic Supplementary Material (ESI) for Journal of Materials Chemistry A.

Supporting Information

for

A Low-Cost Mg^{2+}/Na^{+} Hybrid Aqueous Battery

Xi Cao, Lulu Wang, Jitao Chen*, and Junrong Zheng*

College of Chemistry and Molecular Engineering, Beijing National Laboratory for Molecular Sciences, Peking University, Beijing 100871, China

*To whom correspondence should be addressed at:

E-mail: junrong@pku.edu.cn (J.Z.); chenjitao@pku.edu.cn

Table S1 Comparison of the electrochemical performance of aqueous batteries between this work and the previous reports.

Cell type	Average potential (V)	Cycle Stability	Energy density(Wh·kg^{-1})	Ref.
$Na_{0.44}MnO_2$//$NaTi_2(PO_4)_3$	0.1–1.4	> 50%(1600) at 7 C	33	1
$Na_3MnTi(PO_4)_3$// $Na_3MnTi(PO_4)_3$	1.4	98% (100) at 1 C	40	2
$Na_3V_2(PO_4)_3$// $NaTi_2(PO_4)_3$	1.2	50% (50) at 10 A·g^{-1}	36	3
$Na_2NiFe(CN)_6$// $NaTi_2(PO_4)_3$	1.27	88% (250) at 5 C	42.5	4
$Na_{0.95}MnO_2$//Zn	1.4	92% (1000) at 4 C	78	5
$Na_3V_2(PO_4)_3$//Zn	1.42	77% (200) at 0.5 C	112	6
NiHCF//Zn	1.5	81% (1000) at 0.5A A·g^{-1}	63.9	7
$NaMnO_2$// $NaTi_2(PO_4)_3$	1.15	75% (500) at 5C	30 Wh·kg^{-1} at 50 W·kg^{-1} 20 Wh·kg^{-1} at 1 kW·kg^{-1}	8
Na-birnessite// $NaTi_2(PO_4)_3$	1.4	94% (1000) at 10C	39mAh·g^{-1} at 1C	9
$Na_{0.66}[Mn_{0.66}Ti_{0.34}]$// $NaTi_2(PO_4)_3$	1.2	89% (300) at 2C	76 mAh·g^{-1} at 2C (based on the cathode only)	10
Mn_3O_4// $NaTi_2(PO_4)_3$	**1.2**	**94% (6000) at 10C**	**47 Wh·kg^{-1} at 48 W·kg^{-1}** **23.6 Wh·kg^{-1} at 400 W·kg^{-1}**	**This work**

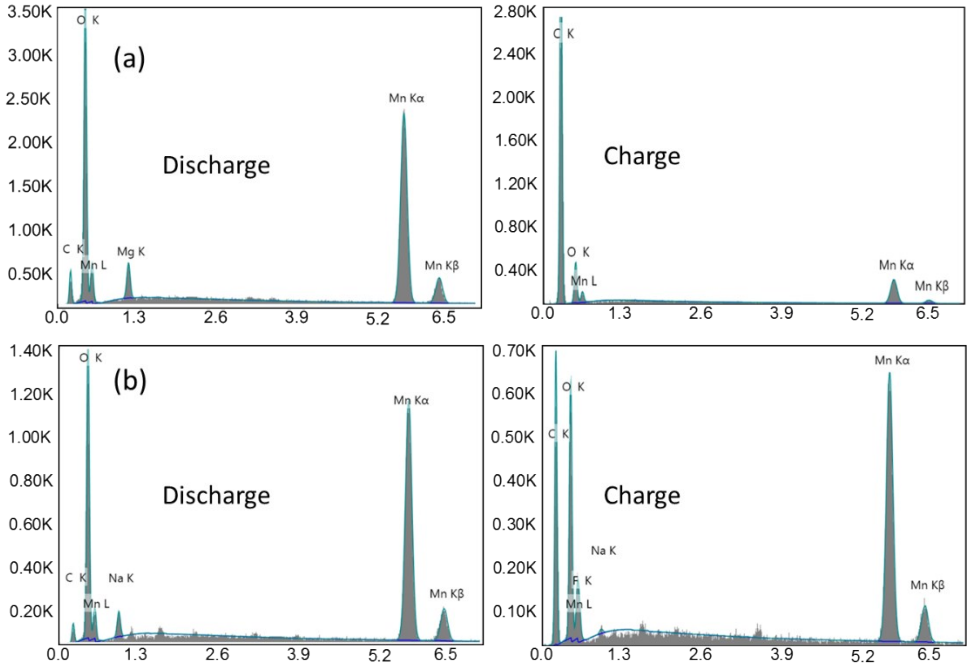

Figure S1. EDS results of the cathode after discharge and charge in a) 2M $MgSO_4$. b) 1M Na_2SO_4.

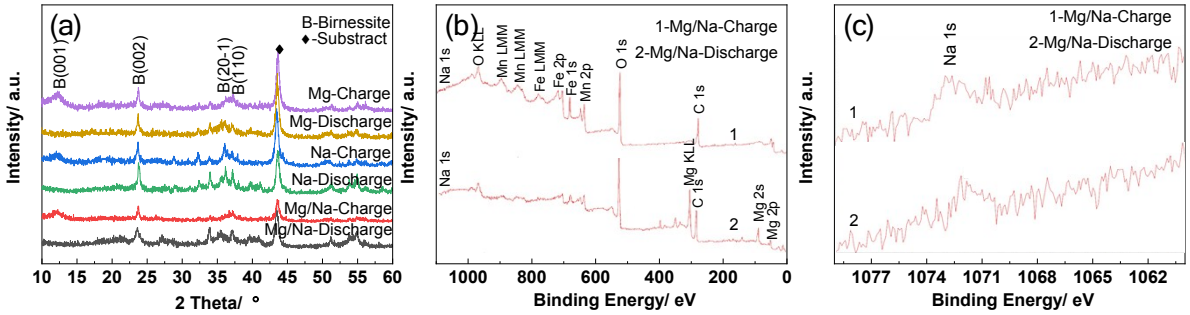

Figure. S2 a)XRD patterns of the cathode after charge/discharge in 2M $MgSO_4$, 1M Na_2SO_4, and 2M $MgSO_4$-1M Na_2SO_4 hybrid electrolytes. b)c) XPS spectra of the cathode after charge and discharge in the hybrid electrolytes.

Besides the EDS and CV studies, we also conduct the XRD and XPS characterization to reveal the insertion/extraction mechanism of Mg^{2+}/Na^{+}. The XRD patterns of the cathode after charge or discharge in 2M $MgSO_4$, 1M Na_2SO_4, and 2M $MgSO_4$-1M Na_2SO_4 hybrid electrolytes are shown in **Fig. S2a**, almost all patterns after charge exhibit the CV peaks corresponding to Birnessite MnO_2 with obvious (001), (002) and (110) peaks. The (001) peak disappears after the discharge, but the (002) peak is still preserved, suggesting that a new lattice arrangement after cations insertion still maintains the (002) plane regularity (in consistent with previous reports[11]), which further confirms the phase change mechanism during charge and discharge.

By comparing the XPS spectra of the cathode after charge and discharge in the hybrid electrolytes, as shown in **Fig. S2b&c**, we can obtain the same results with the EDS results, that is, after the charge process, Na but not Mg could be found; while after the discharge, both Na and Mg could be found in the cathode.

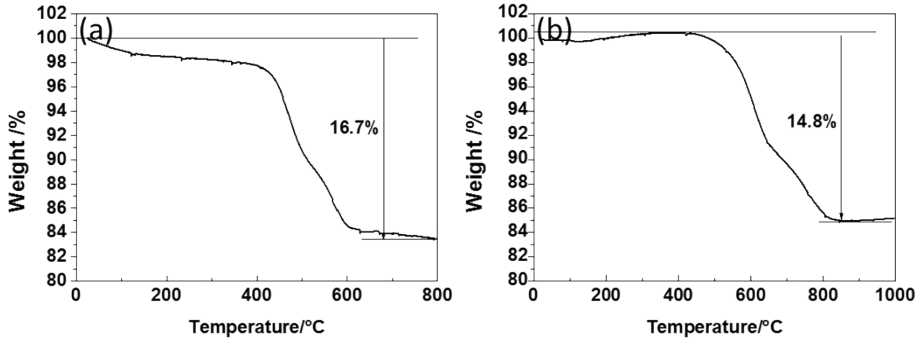

Figure S3. TGA results of a) $NaTi_2(PO_4)_3$-G-C and b) $NaTi_2(PO_4)_3$-S

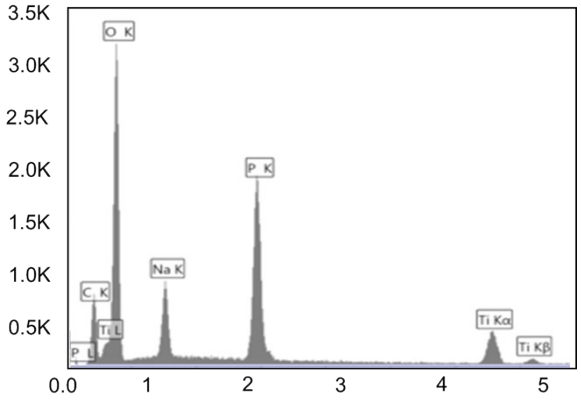

Figure S4. EDS results of $NaTi_2(PO_4)_3$-G-C after cycling in $MgSO_4$ electrolytes.

EDS results of $NaTi_2(PO_4)_3$-G-C after cycling in $MgSO_4$ electrolytes are shown in **Fig. S4,** there is no Mg content detected, indicating very few Mg^{2+} inserting into $NaTi_2(PO_4)_3$.

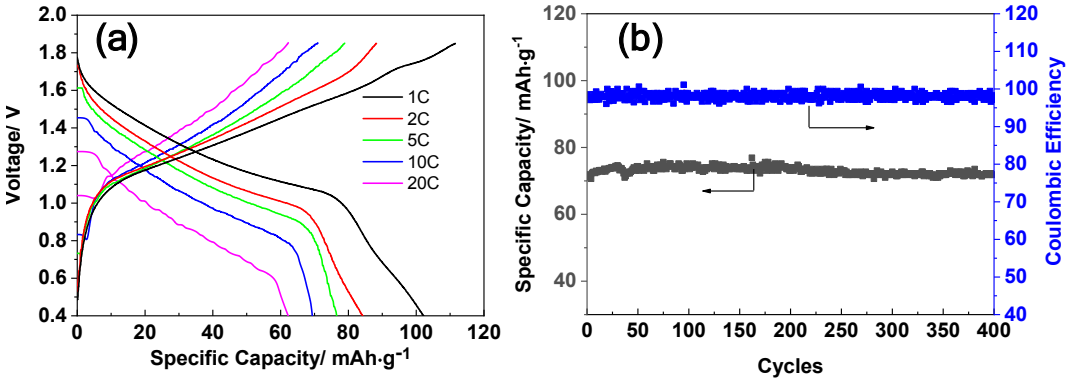

Figure. S5 a) The charge/discharge profiles of Mn_3O_4// $NaTi_2(PO_4)_3$-G-C after the half cell in

hybrid electrolytes at different current rates. b) The cycling performance of Mn_3O_4// $NaTi_2(PO_4)_3$-G-C after the half cell at 10 C

The electrochemical performance of the full cell constructed by Mn_3O_4 and $NaTi_2(PO_4)_3$-G-C after cycling for 30 cycles in three electrode cell is also studied, as shown in **Fig.S5**. The charge and discharge profiles of this full cell at different current densities are shown in **Fig.S5a**. As we can see, the specific capacity of the full cell (based on the anode) reaches 102.3, 84, 76, 68 and 62 $mAh \cdot g^{-1}$ at from 1C to 20 C, which is similar to the full cell using Mn_3O_4 and $NaTi_2(PO_4)_3$-G-C directly. The cycling performance of this full cell at 10C is shown in **Fig.S5b**, the specific capacity shows no obvious decrease after 400 cycles, also suggesting a good stability.

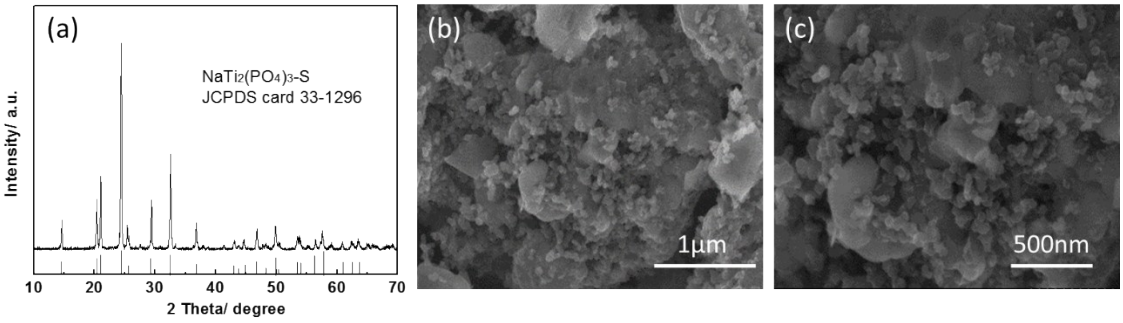

Figure S6. a) T X-ray diffraction pattern of $NaTi_2(PO_4)_3$-S. b) c) SEM image of $NaTi_2(PO_4)_3$-S.

The crystal structure of NTP-S is confirmed by the X-ray diffraction pattern in **Fig. S6,** with all diffraction peaks agreeing well with standard $NaTi_2(PO_4)_3$ without impurity peaks. The detailed morphology of $NaTi_2(PO_4)_3$-S is shown in **Fig. S6b&c.** The $NaTi_2(PO_4)_3$ particles are approximately 300 nm in diameter and are encapsulated by carbon, which is intimately mixed with the precursors. This result shows that this simple solid state synthetic route is sufficient for producing $NaTi_2(PO_4)_3$ with the desired crystalline structure. The carbon did not burn off during

the high-temperature calcining step and instead encapsulated the $NaTi_2(PO_4)_3$ particles, which is the desired outcome. The carbon content in **$NaTi_2(PO_4)_3$-S** is determined to be 14.8 % by the TGA analysis, as shown in **Fig. S3b**.

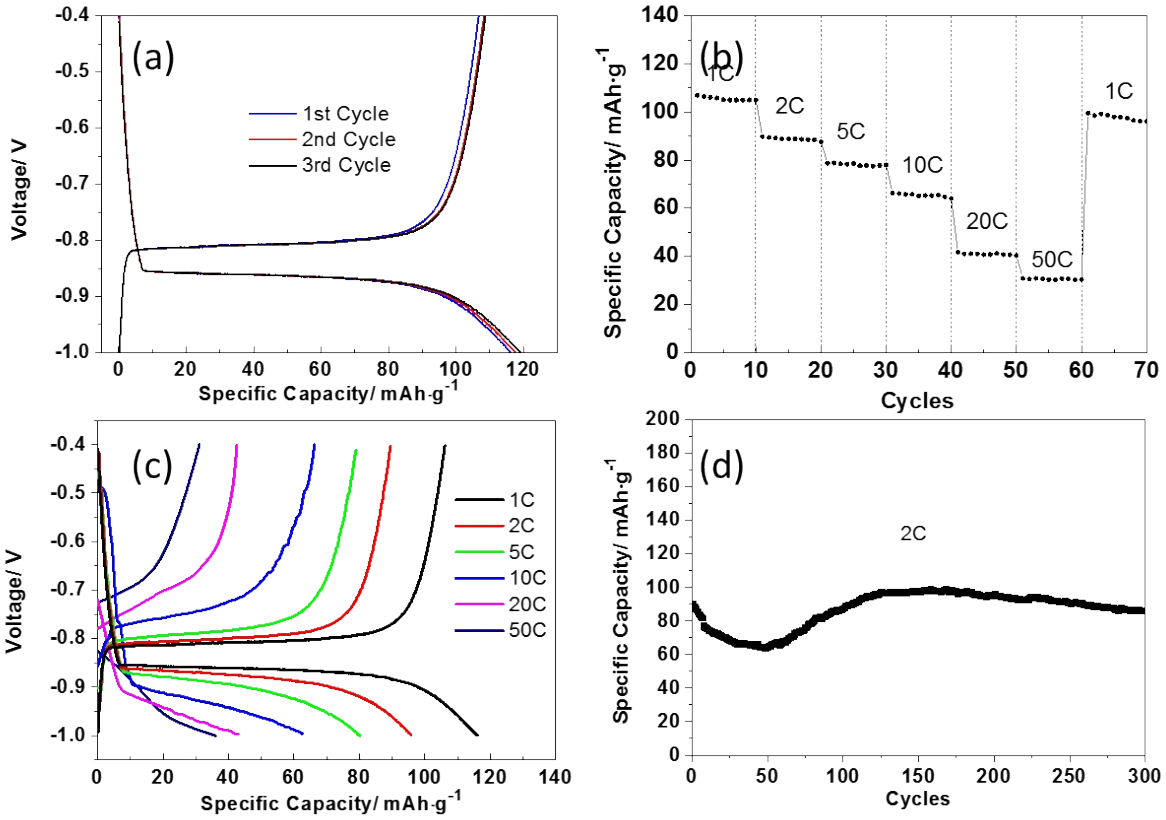

Figure S7. a) Galvanostatic charge and discharge measurement of $NaTi_2(PO_4)_3$-S. b) c) Rate performance. d) Cycling performance at the current density of 2 C.

The electrochemical behavior of $NaTi_2(PO_4)_3$-S in 2M $MgSO_4$-1M Na_2SO_4 hybrid electrolytes is also studied by galvanostatic charge-discharge in the potential range from −1.0 to -0.4 V. As displayed in **Fig. S7a,** similar to the $NaTi_2(PO_4)_3$-G-C, a clear discharge/charge voltage plateau at a potential of around -0.86 V/-0.81 vs. Ag/AgCl can be observed, with the charge and discharge capacity is approximately 108 and 118 $mAh \cdot g^{-1}$ at the current density of 1C, respectively.

With increasing the current density, the specific capacities decrease to 79.0, 66.2 and 41.7 mAh·g^{-1} at the rates of 5, 10 and 20 C, respectively. When the current density decreases to 1C, the capacity goes up to about 96 mAh·g^{-1}, indicating the good rate capability, as shown in **Fig. S7b**. Although the high rate capability of $NaTi_2(PO_4)_3$-S is slightly inferior than that of $NaTi_2(PO_4)_3$-G-C, $NaTi_2(PO_4)_3$-S also exhibits excellent cycling performance at low rates. As shown in **Fig. S7d,** $NaTi_2(PO_4)_3$-S electrode shows a reversible capacity of about 86 mAh·g^{-1} after 300 cycles at the current density of 2 C. The difference in the rate capability of these two anode materials can be attributed to the difference in the nano structure. The size of the NTP nanoparticles in $NaTi_2(PO_4)_3$-G-C is much smaller than that in $NaTi_2(PO_4)_3$-S, and the chemical bonding between the NTP nanoparticles and conductive rGO is tighter than that in $NaTi_2(PO_4)_3$-S. Both contribute to a higher conductivity of the whole composite.

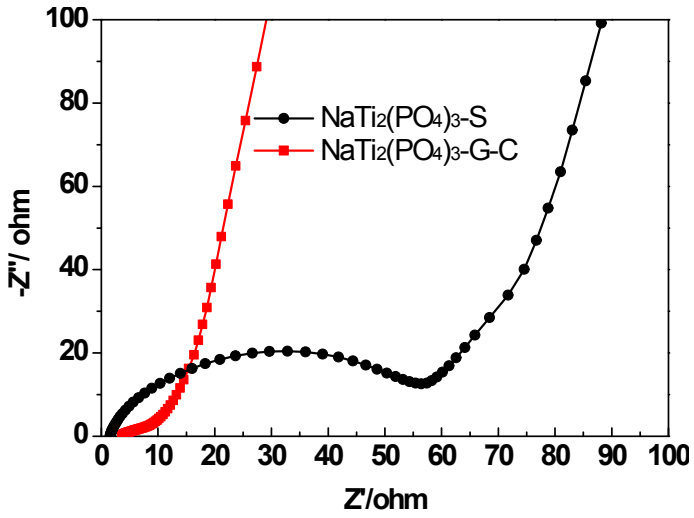

Figure S8. Nyquist plots of the $NaTi_2(PO_4)_3$-G-C and $NaTi_2(PO_4)_3$-S electrodes after 30 cycles.

EIS measurement is performed over a frequency range of 100 kHz to 0.01 Hz to explain the electrochemical difference between the $NaTi_2(PO_4)_3$-G-C and $NaTi_2(PO_4)_3$-S. **Fig. S8** shows the

Nyquist plots of the $NaTi_2(PO_4)_3$-G-C and $NaTi_2(PO_4)_3$-S electrodes after 30 cycles (at 1C). Both profiles display a depressed semicircle in the high frequency region associated with the combined process of surface film (R_f) and the charge transfer resistance (R_{ct}), and a long slope line represents the Warburg impedance (Z_W) at low frequency. As we can see, it is obvious that the R_f and R_{ct} of $NaTi_2(PO_4)_3$-G-C are much smaller than those of the $NaTi_2(PO_4)_3$-S, which indicates a higher conductivity.

1. Z. Li, D. Young, K. Xiang, W. C. Carter and Y. M. Chiang, *Advanced Energy Materials*, 2013, **3**, 290-294.
2. H. Gao and J. B. Goodenough, *Angewandte Chemie*, 2016, **128**, 12960-12964.
3. Q. Zhang, C. Liao, T. Zhai and H. Li, *Electrochim. Acta*, 2016, **196**, 470-478.
4. X. Wu, Y. Cao, X. Ai, J. Qian and H. Yang, *Electrochem Commun*, 2013, **31**, 145-148.
5. B. Zhang, Y. Liu, X. Wu, Y. Yang, Z. Chang, Z. Wen and Y. Wu, *Chemical Communications*, 2014, **50**, 1209-1211.
6. G. Li, Z. Yang, Y. Jiang, W. Zhang and Y. Huang, *Journal of Power Sources*, 2016, **308**, 52-57.
7. K. Lu, B. Song, J. Zhang and H. Ma, *Journal of Power Sources*, 2016, **321**, 257-263.
8. Z. G. Hou, X. N. Li, J. W. Liang, Y. C. Zhu and Y. T. Qian, *Journal of Materials Chemistry A*, 2015, **3**, 1400-1404.
9. X. Q. Zhang, Z. G. Hou, X. N. Li, J. W. Liang, Y. C. Zhu and Y. T. Qian, *Journal of Materials Chemistry A*, 2016, **4**, 856-860.
10. Y. S. Wang, L. Q. Mu, J. Liu, Z. Z. Yang, X. Q. Yu, L. Gu, Y. S. Hu, H. Li, X. Q. Yang, L. Q. Chen and X. J. Huang, *Advanced Energy Materials*, 2015, **5,** 1501005.
11. K. W. Nam, S. Kim, S. Lee, M. Salama, I. Shterenberg, Y. Gofer, J.-S. Kim, E. Yang, C. S. Park, J.-S. Kim, S.-S. Lee, W.-S. Chang, S.-G. Doo, Y. N. Jo, Y. Jung, D. Aurbach and J. W. Choi, *Nano letters*, 2015, **15**, 4071-4079.